On the Differences in Storm Rainfall from Hurricanes Isidore and Lili. Part I: Satellite Observations and Rain Potential

HAIYAN JIANG AND JEFFREY B. HALVERSON

Joint Center for Earth Systems Technology, University of Maryland, Baltimore County, Baltimore, and Meososcale Atmospheric Processes Branch, NASA Goddard Space Flight Center, Greenbelt, Maryland

JOANNE SIMPSON

Laboratory for Atmospheres, NASA Goddard Space Flight Center, Greenbelt, Maryland

(Manuscript received 28 September 2005, in final form 16 May 2007)

ABSTRACT

It has been well known for years that the heavy rain and flooding of tropical cyclones over land bear a weak relationship to the maximum wind intensity. The rainfall accumulation history and rainfall potential history of two North Atlantic hurricanes during 2002 (Isidore and Lili) are examined using a multisatellite algorithm developed for use with the Tropical Rainfall Measuring Mission (TRMM) dataset. This algorithm uses many channel microwave data sources together with high-resolution infrared data from geosynchronous satellites and is called the real-time Multisatellite Precipitation Analysis (MPA-RT). MPA-RT rainfall estimates during the landfalls of these two storms are compared with the combined U.S. Next-Generation Doppler Radar (NEXRAD) and gauge dataset: the National Centers for Environmental Prediction (NCEP) hourly stage IV multisensor precipitation estimate analysis. Isidore produced a much larger storm total volumetric rainfall as a greatly weakened tropical storm than did category 1 Hurricane Lili during landfall over the same area. However, Isidore had a history of producing a large amount of volumetric rain over the open gulf. Average rainfall potential during the 4 days before landfall for Isidore was over a factor of 2.5 higher than that for Lili. When using the TRMM-based MPA-RT rainfall estimate, results are consistent with a previous study, which analyzed just the infrared-based rain estimation; that is, the rain potential history could be used as a predictor for the storm's potential for inland flooding 3–4 days in advance of landfall.

1. Introduction

The combination of rain and freshwater flooding is the number one cause of death from hurricanes in the United States (Elsberry 2002). One goal of the U.S. Weather Research Program (USWRP; Elsberry and Marks 1999) is to improve 72-h quantitative precipitation forecasts of hurricanes for inland flooding. Over oceans, tropical cyclone rainfall is well correlated with storm intensity. From a statistical study of 260 tropical cyclones during 1998–2000, Lonfat et al. (2004) showed that the maximum azimuthally averaged rainfall rate is about 12 mm h^{-1} for category 3–5 hurricanes, but decreases to 7 mm h^{-1} for category 1–2 storms, and to 3 mm h^{-1} for tropical storms. Paradoxically, the heavy rain and flooding of hurricanes over land are not well correlated with the storm maximum wind intensity. Some of the most devastating floods are produced by tropical systems in the weak end of the spectrum, for example, Tropical Storm Claudette [1979, 42 in. of rain $(24\ h)^{-1}$] and Tropical Storm Allison (2001, $6 billion in damages, 27 deaths, 35–40 in. of rain), both impacting the U.S. Gulf coast. It is necessary to identify better methods for quantifying the freshwater threat during tropical cyclone landfalls.

Griffith et al. (1978) proposed a technique to rank storms by their "wetness." The parameter that identifies the storm's wetness is called rain potential, which is defined by using an estimated average rain rate derived from infrared (IR) satellite observations, combined with the storm size and translation speed information.

Corresponding author address: Dr. Haiyan Jiang, Dept. of Meteorology, University of Utah, Rm. 819 WBB, 135 S 1460 E, Salt Lake City, UT 84112.
E-mail: h.jiang@utah.edu

DOI: 10.1175/2007WAF2005096.1

The rainfall potential histories of a dozen tropical cyclones approaching landfall were examined. Griffith et al.'s method correctly predicted the highest actual rainfall totals for the major flooding of Hurricanes Agnes (1972) and Fifi (1974), and the lowest rainfall totals for the relatively dry Hurricanes Celia (1970) and Edith (1971).

It is well known that geosynchronous IR observations have the advantage of high time resolution but lack a strong physical connection between cloud-top temperatures and the surface rainfall (Adler et al. 1993). Use of IR-based techniques also has shown a tendency to overestimate rainfall in areas of cold cirrus and underestimate the rain contribution from warmer-topped, tropical maritime clouds (Barrett 1999). Alternatively, the physical connection between microwave observations from polar-orbiting satellites and precipitation is much better. A technique similar to Griffith et al.'s (1978) rain potential approach is called the tropical rainfall potential (TRaP), which was developed at the National Oceanic and Atmospheric Administration/National Environmental Satellite, Data, and Information Service (NOAA/NESDIS; Kidder et al. 2005; Ferraro et al. 2005). TRaP uses the Special Sensor Microwave Imager (SSM/I), the Advanced Microwave Sounding Unit (AMSU), and the Tropical Rainfall Measurement Mission (TRMM) Microwave Imager (TMI) rain rates to predict tropical cyclone rainfall potential. Ferraro et al. (2005) found that the TMI TRaPs performed the best when compared to the AMSU and SSM/I TRaPs.

However, the sampling imposed by the low-orbit microwave observations is poor. There have been recent efforts to combine the IR and microwave observations to provide better precipitation estimates at improved spatial and temporal resolutions (Adler et al. 1993, 1994, 2003; Huffman et al. 2001). In the framework of the TRMM project, the National Aeronautic and Space Administration (NASA) real-time Multisatellite Precipitation Analysis (MPA-RT) has produced gridded 3-h precipitation rate estimates with relatively high horizontal resolution ($0.25° \times 0.25°$ latitude–longitude) since January 2002. These rainfall estimates are based on microwave information provided by various low-orbiting satellites, merged with IR-based estimates from geostationary meteorological satellites (Huffman et al. 2003, 2007). TRMM products are used to calibrate the estimates. In this paper, we will incorporate Griffith et al.'s (1978) rain potential technique into the new MPA-RT data for two tropical cyclones (Isidore and Lili) that made landfall on the U.S. Gulf coast during 2002.

Section 2 presents a description of MPA-RT data, the definition of rain potential, and the method used to analyze the MPA-RT rainfall parameters. Since the MPA-RT product is relatively new, very few validation studies (Katsanos et al. 2004) have been published in the literature—none for severe weather events like hurricanes. Section 2 will also include an evaluation of the MPA-RT data by comparing the satellite precipitation estimates for Isidore and Lili against the available combined U.S. Next-Generation Doppler Radar (NEXRAD; 10-cm Doppler radars operated by the National Weather Service) and gauge measurements over the U.S. Gulf coast. Section 3 provides a synoptic overview of Isidore and Lili. Sections 4 and 5 present the results of the rainfall history and the rain potential difference of the two storms. Section 6 summarizes the work and section 7 addresses prospects for future research.

2. Data and methodology

a. MPA-RT data

The MPA-RT precipitation estimates used in this study are provided by two different sets of sensors. Microwave data are collected by various low-orbit satellites, including TMI, SSM/I, the Advanced Microwave Scanning Radiometer for the Earth Observing System (AMSR-E), and AMSU. Precipitation estimates are made from TMI, SSM/I, and AMSR-E microwave data by applying the Goddard Profiling Algorithm (GPROF; Kummerow et al. 1996). AMSU microwave measurements are converted to rainfall estimates by using the AMSU-B algorithm (Zhao and Weng 2002; Weng et al. 2003). The IR data are collected by the international constellation of Geosynchronous Earth Orbit (GEO) satellites. The microwave estimates are calibrated using the TMI, and IR estimates are calibrated with the microwave estimates. The microwave and GEO-IR estimates are merged in a probability-matched method (Huffman et al. 2003, 2007). A near-real-time product (so-called MPA-RT) that only depends on microwave and infrared data is computed a few hours after the acquisition of data from the orbiting platforms. The MPA-RT dataset consists of gridded precipitation rate files with $0.25° \times 0.25°$ latitude–longitude horizontal resolution, within the global latitude belt 60°S–60°N. The temporal resolution is 3 h and the files are generated on synoptic observations times (0000, 0300, . . . , 2100 UTC). A post-real-time product called MPA is produced from a merged microwave–IR dataset that, in postprocessing mode, is calibrated using the TRMM Combined Instrument (TCI). The TCI utilizes the superior horizontal resolution of the TMI and TRMM Precipitation Radar (PR) to produce a high-quality merged microwave rainfall estimate. In this

study, only the real-time MPA-RT product is used because our purpose is to examine the predicting capability of the rainfall potential derived from satellite observations. For this study, TRMM version 6 of the post-real-time MPA rain estimates for Isidore and Lili are compared with MPA-RT estimates for these two storms and no significant differences are found.

To verify the MPA-RT product, rain estimates of MPA-RT during the landfall of Isidore and Lili are compared to the stage IV National Centers for Environmental Prediction (NCEP) Multisensor Precipitation Estimator (MPE IV) product. The Office of Hydrology Development (OHD) of the National Weather Service (NWS) has developed the MPE precipitation estimation application and has deployed it at Weather Forecast Offices (WFOs) and River Forecast Centers (RFCs) throughout the nation. The MPE combines radar rainfall estimates with rain gauge measurements and produces a suite of multisensor rainfall estimates. Radar biases are adjusted prior to the MPE analysis by the technique developed by Smith and Krajewski (1991). The analysis scheme used in MPE products utilizes optimal estimating theory (Seo 1998), which optimally estimates rainfall fields using rain gauge and radar data under partial data coverage conditions. By objectively taking the spatial coverage into account, more accurate estimates of rain versus no-rain areas are obtained. The MPE IV product provides rainfall estimates that are gridded into a national product from the regional hourly/6-hourly MPE analyses produced by the 12 RFCs. The manual quality control performed at the RFCs is contained in the MPE IV 6- and 24-h rainfall accumulation estimates. The horizontal resolution of the MPE IV dataset is 4 km $\times$ 4 km on a local polar stereographic grid. MPE IV data since January 2002 are archived at a dedicated NCEP Web page (http://wwwt.emc.ncep.noaa.gov/mmb/ylin/pcpanl/stage4/).

In this study, the MPA-RT satellite precipitation estimates are validated against the MPE IV radar + gauges data for Isidore's landfall period (starting at the U.S. landfall time and extending several days past that time) during 24–28 September 2002 and Lili's landfall period during 3–5 October 2002. The spatial pattern comparison is made for the precipitation accumulated on the whole time period of landfall (5 days for Isidore, 3 days for Lili), while the statistical comparison is made for the precipitation accumulated on 24-h intervals. We choose the 24-h interval instead of 3 h for the following reasons. 1) The central goal of this study is to estimate the rainfall potential from MPA-RT data, and the rainfall potential defined here is a daily mean parameter. 2) MPE IV contains 1-, 6-, and 24-h rainfall accumulations. No manual quality control is done for hourly MPE IV data. 3) Due to the poor sampling of the microwave data, unrealistic oscillations are common in the 3-h time series of the MPA-RT rainfall history and a smoothing over a 12- or 24-h period is necessary to remove some artifacts. For the verification procedure, the MPE IV estimate grid boxes whose centers fall within the MPA-RT 0.25° $\times$ 0.25° latitude–longitude boxes are averaged. Within the MPE IV spatial coverage, the mean daily rainfall amounts for MPE IV and MPA-RT are calculated.

Figure 1 shows the contours of 5-day rain accumulation from MPE IV and MPA-RT during Isidore's landfall (1200 UTC 23 September–1200 UTC 28 September 2002) and 3-day rain accumulation from MPE IV and MPA-RT during Lili's landfall (1200 UTC 3 October–1200 UTC 5 October 2002). It is clearly seen in the figure that the MPE IV and MPA-RT rain accumulation fields are generally similar in areal extent (within the NEXRAD and gauge spatial coverage) and magnitude. However, an overestimate by MPA-RT is obvious in the heavy rain regions for both storms. (Note that there was no MPE IV coverage in the very heavy rainfall region of Isidore over the Yucatan.) To illustrate the comparison of MPA-RT and MPE IV rain estimates point by point, Fig. 2 presents the scatterplot of MPA-RT-derived and MPE-IV-analyzed daily rain rates during the landfalls of Isidore and Lili, respectively. The correlation coefficient is 0.84 for Isidore and 0.75 for Lili. Considering the very different sample volumes among the satellite remote sensing instruments, ground-based radars, and rain gauges, the correlations are relatively good. However, for daily rainfall larger than 10 mm day^{-1} data points, MPA-RT produces a general overestimate. The overall positive biases of MPA-RT are 2.38 and 0.49 mm day^{-1} for Isidore and Lili, respectively. Because Isidore's rain during landfall is much heavier than Lili's, the positive bias of MPA-RT for Isidore is much larger than that for Lili.

These validation results show that the MPA-RT product makes a reasonable rainfall estimate for tropical cyclones after comparing with MPE IV data during Isidore's and Lili's landfall. A 10%–30% overestimate is seen for MPA-RT rain relative to MPE IV rain. This is consistent with previous studies on microwave rainfall retrieval validation (Adler et al. 2000; Nesbitt et al. 2004). The reason is threefold. 1) Passive microwave rainfall algorithms over land generally are based on the observation that precipitation-size ice particles (graupel, snowflakes, and hail) suspended in many rain clouds are sufficiently effective microwave scatterers; they therefore depress satellite-observed 85-GHz brightness temperatures relative to the radiometrically

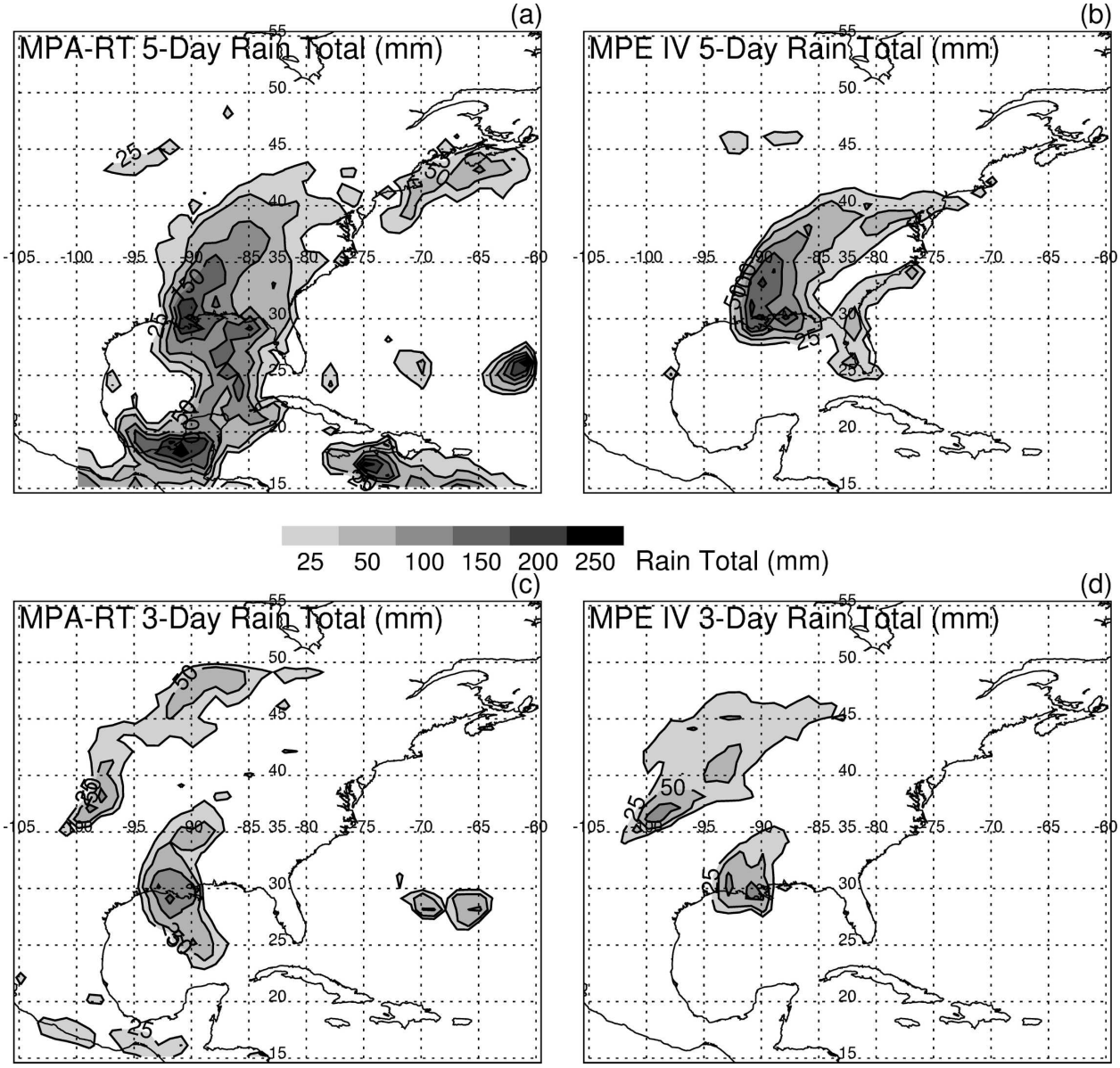

FIG. 1. (a) TRMM MPA-RT and (b) MPE IV 5-day rain accumulation (mm) during Isidore's landfall (1200 UTC 23 Sep–1200 UTC 28 Sep 2002); (c) TRMM MPA-RT and (d) MPE IV 3-day rain accumulation (mm) during Lili's landfall (1200 UTC 3 Oct–1200 UTC 5 Oct 2002).

"warm" land surface background (Spencer et al. 1989). As pointed out by Nesbitt et al. (2004), the microwave-based algorithm has a high bias over land due to the inappropriateness of the empirically derived 85-GHz ice scattering–rain relationship. 2) The radar rain estimate itself could be biased due to some range-dependent factors such as ground clutter, blockage by structures or topography, and beam spreading or attenuation (Conner and Petty 1998). 3) Rain gauge measurements could underestimate the true catch in the large surface wind environment induced by hurricanes.

b. Definition of rain potential

This study adapts the technique proposed by Griffith et al. (1978) to assess the flooding potential of approaching hurricanes using a parameter called the mean total rain potential, defined as

$$\text{mean total rain potential} = \frac{\overline{D}\,\overline{d}}{\overline{v}}, \qquad (1)$$

where $\overline{D}$ is the MPA-RT daily average storm rainfall (mm day^{-1}), $\overline{d}$ the mean cross section (km) of the storm

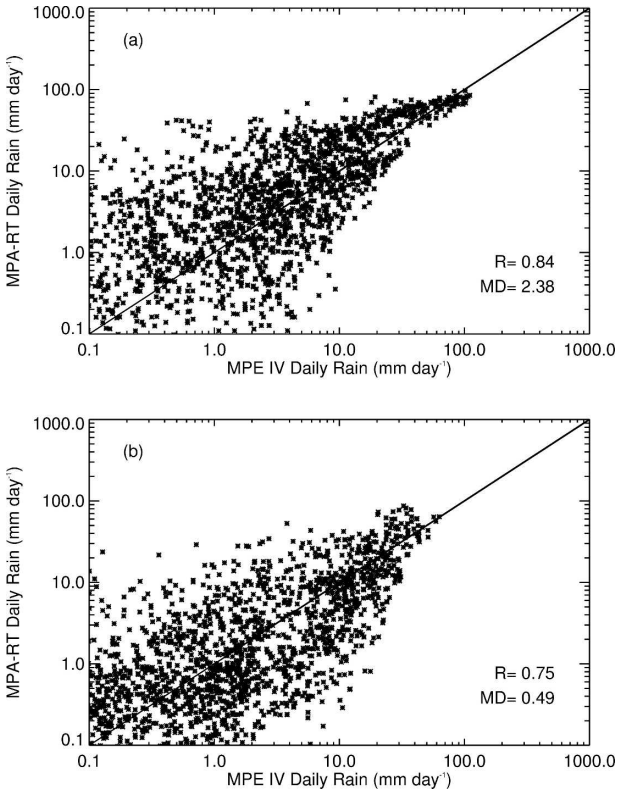

FIG. 2. Comparisons of TRMM MPA-RT-derived and MPE IV-analyzed daily rain rates (mm day^{-1}) during (a) Isidore's and (b) Lili's landfall. Correlation R and mean difference (MD) are indicated.

as measured from the satellite image in the direction of motion ($\overline{d}$ is determined from the MPA-RT daily rain accumulation image, where a line is drawn and measured for the continuous rain area in the direction of the storm motion), and $\overline{v}$ the mean storm translation speed (km day^{-1}) derived from hurricane best-track data obtained from the National Hurricane Center (NHC) 2002 Atlantic hurricane season report. It is taken that the expected duration of rainfall at a point as a tropical cyclone passes overhead is approximately $\overline{d}/\overline{v}$. The mean total rainfall, then, would be $(\overline{D}\,\overline{d})/\overline{v}$. This definition is the same as the TRaP used in Kidder et al. (2005).

c. Analysis method

The MPA-RT rainfall parameters are derived in storm-relative coordinates. The azimuthally mean values are calculated in 28-km-wide annuli around the storm center outward to the 1111-km radius for MPA-RT-derived parameters. The resulting dataset allows us to examine the radial dependence of parameters as a function of time. Inner-core [within 111 km of the tropical cyclone center; Rodgers et al. (1994)] mean parameters can also be computed as the storm evolves.

To examine the storm wetness parameter, the storm total volumetric MPA-RT rain is calculated within the tropical cyclone region. The storm size (i.e., the maximum storm radius) as a function of time is determined from the 3-hourly MPA-RT rainfall images. A combination of automatic and manual methods is used to draw a circle around the storm at the observation time by excluding rain that is not associated with the tropical cyclone (H. Pierce 2005, personal communication). Only pixels inside the circle of the maximum storm radius are counted when calculating the total volumetric parameters (ΣX):

$$\sum X = \sum_{i=0}^{i=n} X_i A, \tag{2}$$

where X represents the MPA-RT rain rate and A is the area of each single pixel. For the MPA-RT rain rate, A is $0.25^\circ \times 0.25^\circ$, while n is the number of data points inside the storm.

In this study, two rain parameters are used. One is rainfall rate, which is the sole parameter that the rainfall intensity is dependent on. The rainfall intensity can give an indication of extreme rainfall amounts over a short period, but does not necessarily correspond to higher flood potential over the course of the storm. The other is storm total volumetric rain, which is dependent on both the rain rate and the storm size. If we replace the area calculation in Eq. (2) with the linear distance in Eq. (1), Eq. (2) will become the numerator of Eq. (1). This indicates that the volumetric rain is the most important parameter to consider for the rainfall potential.

3. Hurricanes Isidore and Lili

Hurricane Isidore (14–27 September 2002) was the 10th Atlantic tropical cyclone of 2002. Isidore formed from a tropical wave along the northern coast of Venezuela on 14 September and moved westward (Fig. 3). It slowly intensified to tropical storm stage as it drifted westward. The system moved very slowly toward the northwest and west-northwest and reached hurricane status on 19 September, making landfall in western Cuba on 20 September as a category 1 hurricane [Saffir–Simpson hurricane scale; Simpson (1976)]. Isidore reached its maximum intensity of 57 m s^{-1} (category 3) at 1800 UTC 21 September and hit the northern Yucatan Peninsula on 22 September. The storm meandered for 24–36 h over the northern Yucatan and weakened to a minimal tropical storm. Isidore made landfall with winds of 28 m s^{-1} west of Grand Isle, Louisiana, at

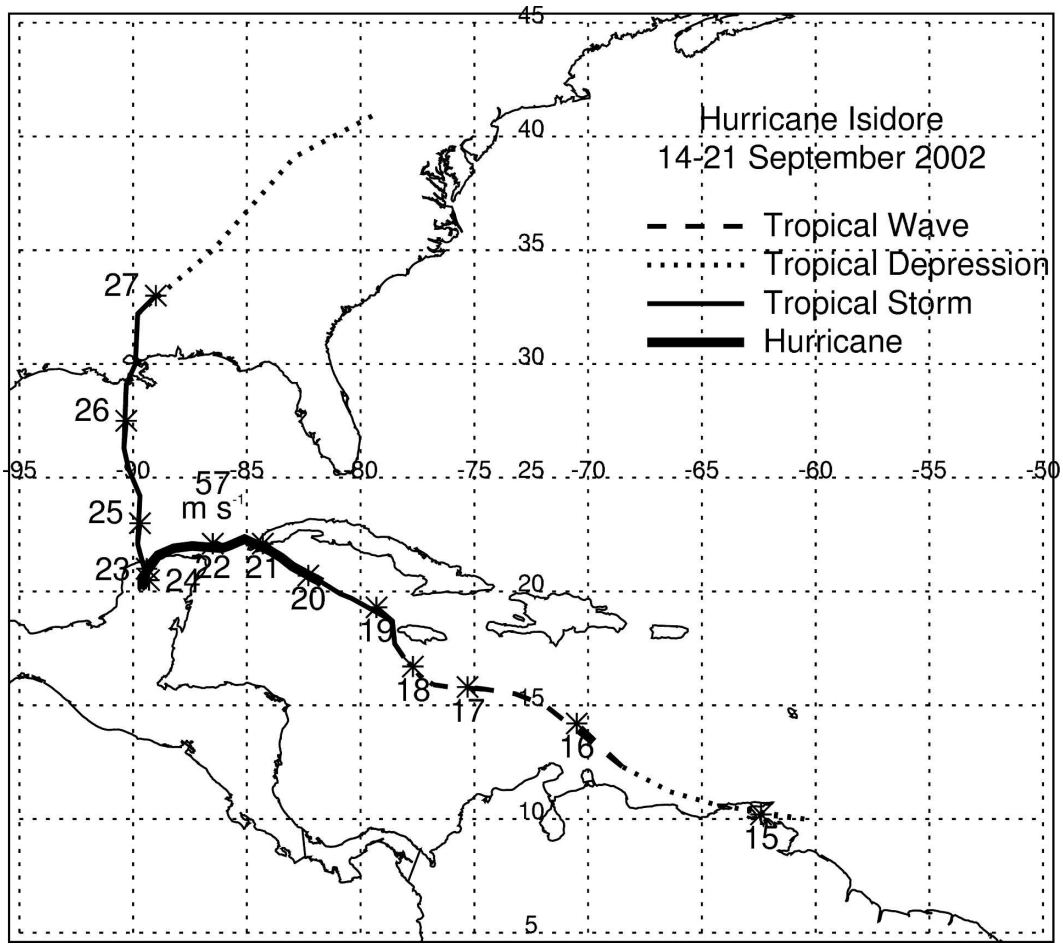

FIG. 3. Best-track location and intensity for North Atlantic Hurricane Isidore (14–27 Sep 2002). The maximum wind speed intensity on 22 Sep is indicated.

0600 UTC 26 September. Once it moved inland, Isidore weakened to a tropical depression and moved north-northeastward across the southeastern United States, producing torrential rains. The maximum storm total rain caused by Isidore's landfall in the United States is 47 cm at New Orleans/Algiers, Louisiana. However, 77.4 cm of storm total rain was measured at Tixmucuy/Campeche, Mexico during 22–24 September 2002.

Hurricane Lili (21 September–4 October 2002) was the 13th Atlantic tropical cyclone of 2002. It formed from a tropical wave 1 week after Isidore's formation over the tropical Atlantic Ocean (Fig. 4). Lili developed into a tropical storm on 23 September and its winds reached 31 m s^{-1} on 24 September. The storm weakened to an open tropical wave on 25–26 September in the east-central Caribbean due to strong vertical wind shear. Lili reintensified and became a hurricane on 30 September while passing over Cayman Brac and Little Cayman Islands. After crossing western Cuba as a category 2 storm, Lili's winds intensified to 64 m s^{-1} (category 4) early on 3 October over the north-central Gulf of Mexico and then rapidly weakened to 41 m s^{-1} (category 1) during the 13 h until its landfall along the Louisiana coast at approximately 1300 UTC 3 October. However, it is an apparent paradox that the category 1 Hurricane Lili produced much less total volumetric rain during its landfall than did Isidore, which made landfall 1 week earlier over the same area as a greatly weakened tropical storm. The highest storm total rain caused by Lili's landfall in the United States is only 21.3 cm at Buras, Louisiana.

4. Time history of rainfall of Isidore and Lili

a. Storm total volumetric rain versus intensity

To estimate the evolution of Isidore and Lili's storm total rain history, the MPA-RT-derived 3-hourly rain rates are integrated for the entire storm volume. Figure 5 shows time series of MPA-RT-derived total storm

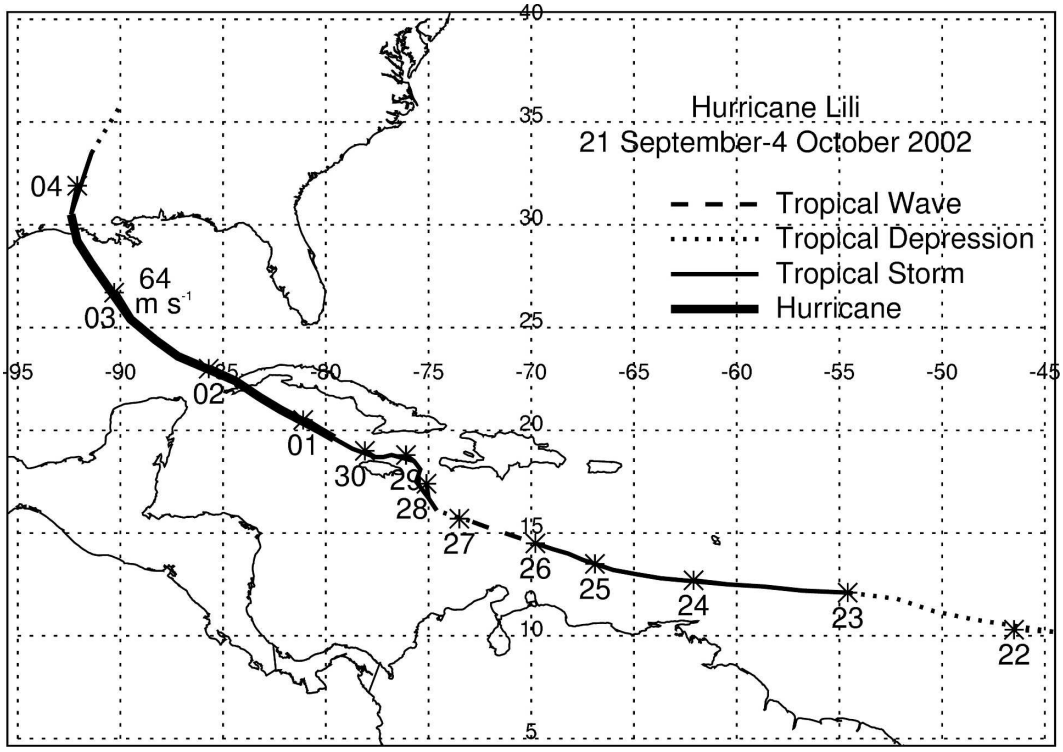

FIG. 4. Best-track location and intensity for North Atlantic Hurricane Lili (21 Sep–4 Oct 2002). The maximum wind speed intensity on 3 Oct is indicated.

volumetric rain and the maximum surface wind speeds for Isidore and Lili, respectively. The time series are filtered by a four-point smoothing method to remove the unrealistic oscillations of the 3-hourly MPA-RT data due to the sampling issue (G. Huffman and H. Pierce 2005, personal communication). It is seen in Fig. 5 that at 3 h after landfall, Isidore's volumetric rain reached its maximum: 4.6 km^3 h^{-1}. In contrast, Lili's

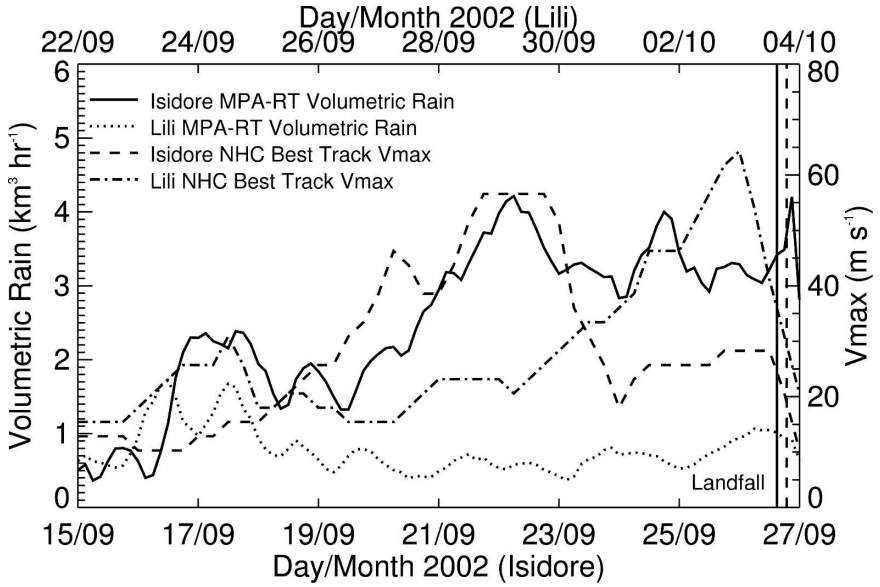

FIG. 5. Time series of Isidore and Lili's intensity (Vmax derived from NHC best-track reports) and MPA-RT volumetric rain. Isidore's (Lili's) landfall is indicated by the vertical solid (dashed) line.

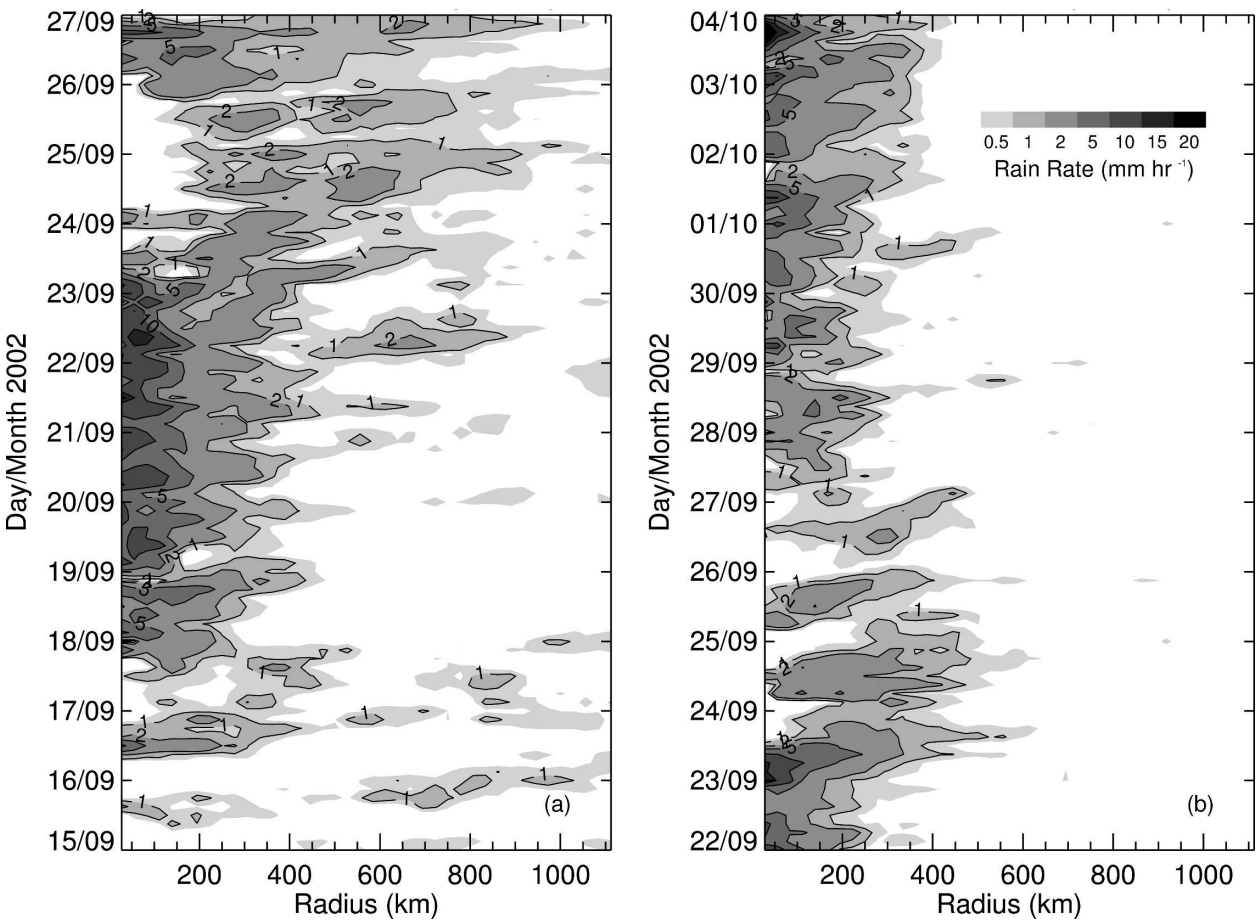

FIG. 6. Time–radius view of (a) Isidore's and (b) Lili's azimuthally averaged MPA-RT-derived rain rates for every 3 h. Rain rates are azimuthally averaged for annuli 28 km in width extending 1111 km outward from the center.

storm volumetric rains during and after landfall were less than 1.6 $km^3\ h^{-1}$. In reviewing the entire life cycle of the two storms, it is found that Isidore's volumetric rains were always much larger than Lili's except for the first 2–3 days of their life cycles. For Isidore, there are four episodes when the storm total volumetric rain increases significantly. These episodes occurred approximately on 16–18, 19–23, 24–25, and 26–27 September. During the second episode, the volumetric rains increased by about 4 $km^3\ h^{-1}$. This episode was coincident with Isidore's period of maximum intensity. During the third and fourth episodes, Isidore's storm total volumetric rains remained large (above 4 $km^3\ h^{-1}$), but its maximum surface winds decreased. This indicates that the volumetric rain totals do not always relate well with storm intensification episodes. However, as we will see in sections 2b and 2c, the rainfall intensity (shown by the inner-core mean rain rate) does relate better with the storm intensification. For Lili, two total volumetric rain episodes could be weakly defined: one was on 24 September, and the other on 3 October. But only about a 1 $km^3\ h^{-1}$ increase in volumetric rains was found during these two episodes, which is much smaller than those for Isidore's total rain episodes. It is also noted that Lili's two total rain episodes were coincident with its two storm intensity maxima.

b. Radial distribution of rain rate

To examine the temporal change of Isidore and Lili's horizontal distribution of rain rates during their entire life cycles, the MPA-RT derived 3-hourly rain rates of Isidore and Lili are azimuthally averaged using the sampling method described in section 2c. The averaged rain-rate values are presented in a time–radius format in Fig. 6. Generally, we see from Fig. 6 that Lili's rain was within a 400-km radius, while Isidore was a relatively large storm with rainbands extending radially out to 1100 km. Starting at 21 September, Isidore's size expanded, and the last three episodes of peak volumetric rain were related to this size increase.

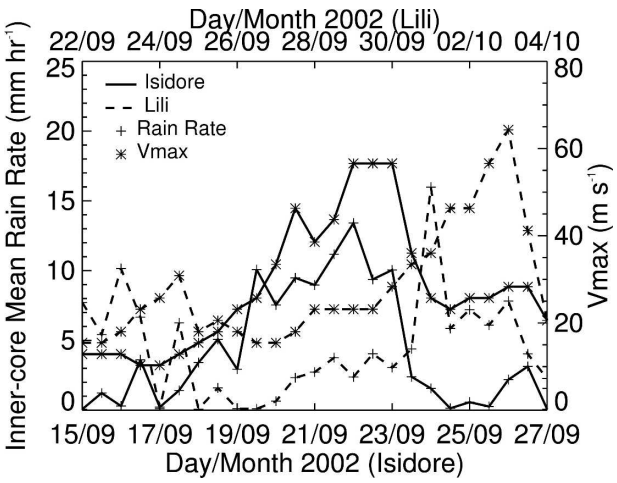

FIG. 7. Time series of Isidore and Lili's intensity (Vmax derived from NHC best-track reports) and MPA-RT-derived inner-core (within 111 km from the storm center) mean rain rate.

From Fig. 5, two maximum surface wind peaks are identified on 20 and 22–23 September for Isidore, and on 24 September and 3 October for Lili, respectively. Inner-core rain maxima are usually seen 1–2 days before the storm intensity peaks from Fig. 6. To investigate if there were convective bursts [a long-lived mesoscale system consisting of a cluster of high cumulonimbus towers within the inner-core region that approaches or reaches the tropopause with nearly undiluted cores; Rodgers et al. (2000)] related to these storm intensity peaks, 3-h IR images are reviewed along with MPA-RT rain rates. As a result, two convective bursts are identified on 18–19 and 21–22 September for Isidore, and on 22–23 September and 1 October for Lili, respectively.

c. Inner-core mean rain rate versus intensity

To show clearer evidence regarding the relationship between storm intensification and convective bursts, Fig. 7 presents a time series of MPA-RT-derived inner-core-averaged rain rates and maximum surface wind speeds for Isidore and Lili. It is seen clearly from Fig. 7 that the convective bursts (inner-core mean rain-rate peaks) appear to precede the times of maximum surface winds. This convective burst (inner-core rain peak) and intensity relationship was also revealed in satellite and aircraft observation studies of Typhoon Bobbie (1992; Rodgers and Pierce 1995), Hurricane Opal (1995; Rodgers et al. 1998), Typhoon Paka (1997; Rodgers et al. 2000), and Hurricane Bonnie (1998; Heymsfield et al. 2001), as well as in observational studies of Hurricane Daisy (1958; Riehl and Malkus 1961) and Tropical Cyclone Oliver (1993; Simpson et al. 1998).

d. Plan view of daily rain accumulation

Figure 8 (Fig. 9) shows the plan views of the distribution of MPA-RT-derived daily rain accumulations for Isidore during 16–27 September (for Lili during 22 September–4 October). From Fig. 8, we see that Isidore's daily rain area was shifted from the northeast to the southeast quadrant of the storm from 16 to 18 September. This period corresponds to the first episode of storm total volumetric rain identified from Fig. 5. Volumetric daily rains increased from 15.4 km^3 day^{-1} on 16 September to 19.7 km^3 day^{-1} on 17 September, and then to 22.1 km^3 day^{-1} on 18 September (Table 1). Rain intensity also increased during this period, which can be seen from the daily mean rain rate values: 11.6, 16.7, and 24.5 mm day^{-1} for 16, 17, and 18 September, respectively (Table 1). Prior to its first landfall in the Yucatan Peninsula on 22 September, Isidore became fairly intense with high rainfall intensity. During the second total volumetric rain episode between 19 and 22 September, the daily mean rain rate (i.e., rain intensity) increased from 23.2 mm day^{-1} on 19 September to 44.9 mm day^{-1} on 21 September. There was a significant amount of rain within the inner-core region of the storm during this period. According to Table 1, for the 3 days before the first landfall in the Yucatan, Isidore's daily mean rain rate averaged around 40 mm day^{-1}, while the daily volumetric rain averaged around 40–45 km^3 day^{-1}. The storm stalled for 24–36 h over the northern Yucatan before moving north back over the Gulf waters. When it remerged into the Gulf, its inner core completely collapsed and the size of the circulation increased dramatically. After interacting with the Yucatan Peninsula, Isidore's daily mean rain rate decreased to about 29 mm day^{-1}, while the volumetric rain increased to over 55 km^3 day^{-1}. These changes reflect the fact that while the intensity of the rain decreased as the inner core of Isidore collapsed, the total amount of rain increased since the size of the storm increased significantly. The storm reached its maximum size on 24 September and became more and more asymmetric afterward. Isidore's rain pattern shifted to the northeast and northwest quadrants after its landfall on 26 September. The daily mean rain rate and total volumetric daily rain reached a second maximum on the landfall day (Table 1) when the storm intensity was still at tropical storm stage. This total rain maximum was produced mainly by Isidore's strong outer rainbands. Due to its large storm size, Isidore produced widespread rains over the eastern United States for 5 days from 24 to 28 September. The 5-day total rain accumulation during Isidore's landfall has a maximum of about 200 mm over Louisiana (Figs. 1a and 1b).

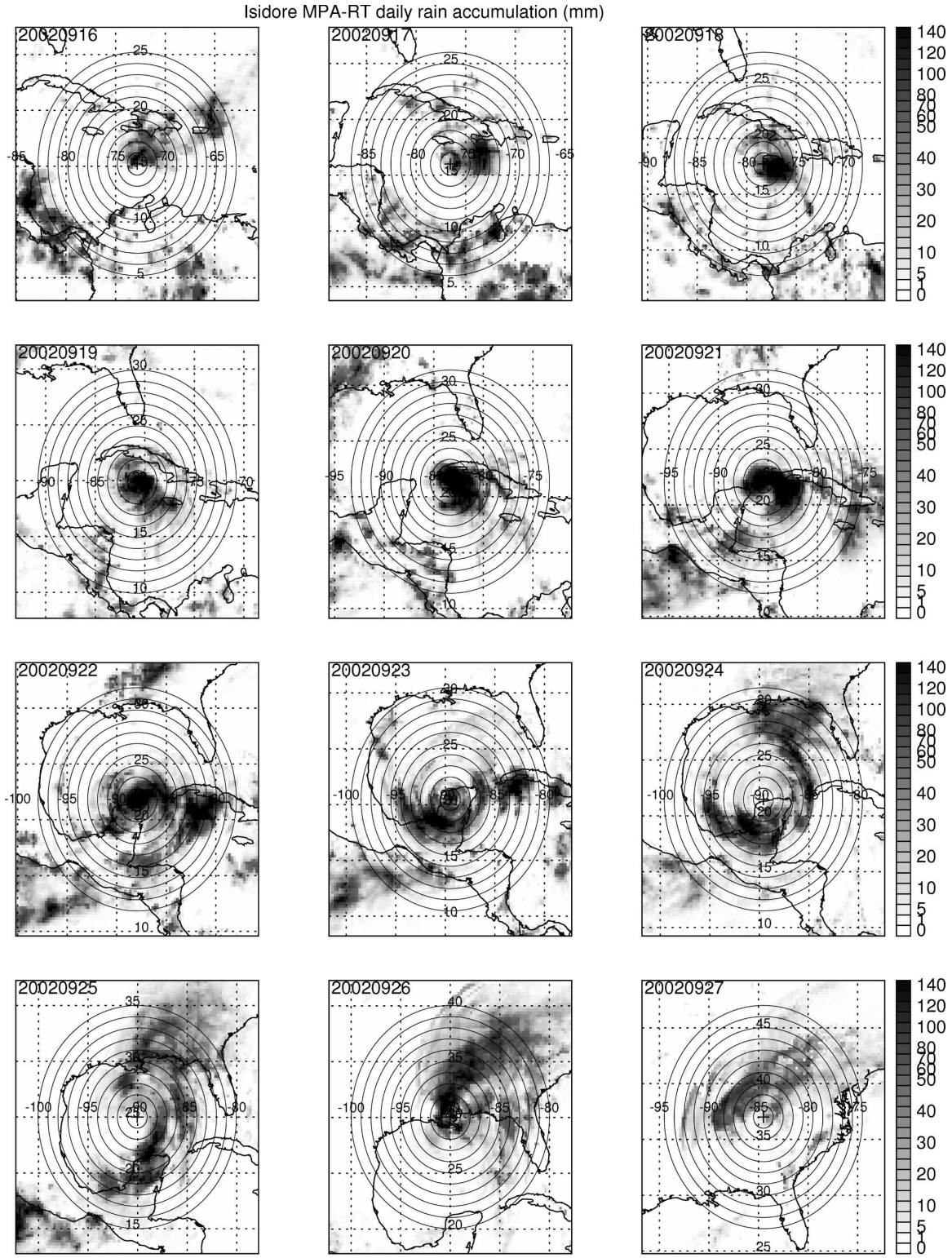

FIG. 8. MPA-RT-derived daily rain accumulations (mm) for Hurricane Isidore between 16 and 27 Sep 2002.

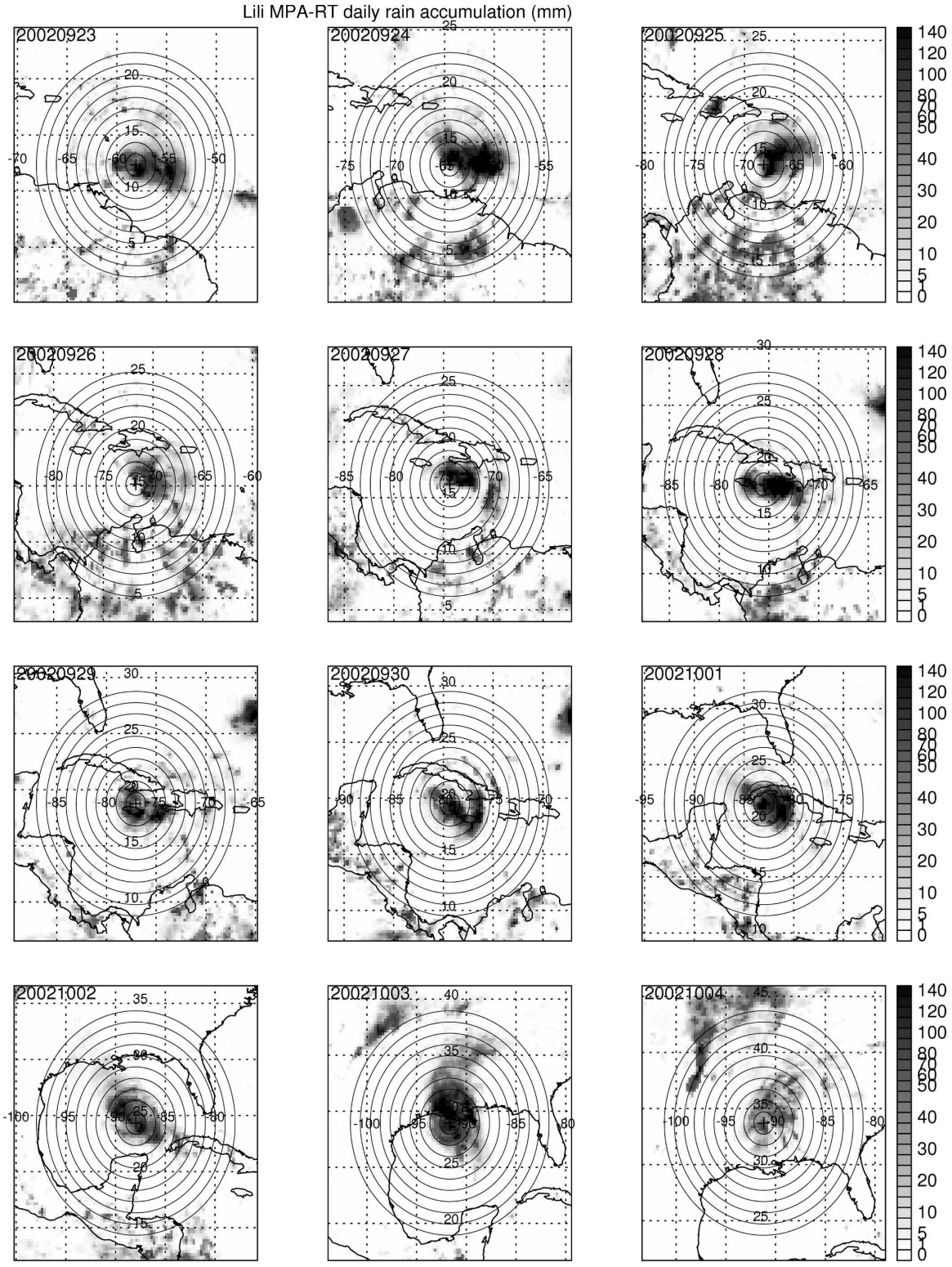

FIG. 9. MPA-RT-derived daily rain accumulations (mm) for Hurricane Lili between 23 Sep and 4 Oct 2002.

TABLE 1. Comparison of daily rain parameters and rain potentials derived from the MPA-RT and GPI products for Isidore and Lili.

Isidore (made landfall on 26 Sep 2002)											
Day (2002)	16 Sep	17 Sep	18 Sep	19 Sep	20 Sep	21 Sep	22 Sep	23 Sep	24 Sep	25 Sep	26 Sep
MPA-RT daily mean rain rate (mm day^{-1})	11.6	16.7	24.5	23.2	37.3	44.9	35.3	29.0	29.9	26.9	30.1
GPI daily mean rain rate (mm day^{-1})	21.5	16.8	21.6	17.7	19.6	21.4	17.8	17.7	18.6	15.2	7.3
MPA-RT daily volumetric rain (km^3 day^{-1})	15.4	19.3	22.1	27.2	34.0	38.0	59.9	50.5	57.6	53.0	58.5
GPI daily volumetric rain (km^3 day^{-1})	24.3	30.2	27.7	43.6	55.9	66.4	58.9	74.6	70.3	65.7	20.0
MPA-RT mean total rain potential (mm)	27.1	71.9	77.1	82.6	169.9	199.1	156.8	279.5	170.2	87.0	79.7
MPA-RT mean total rain potential for 4 days before landfall								173			
GPI mean total rain potential (mm)	51.9	60.4	75.3	61.5	125.2	165.3	87.3	147.9	104.7	46.2	12.0
GPI mean total rain potential for 4 days before landfall								97			
Lili (made landfall on 3 Oct 2002)											
Day (2002)	23 Sep	24 Sep	25 Sep	26 Sep	27 Sep	28 Sep	29 Sep	30 Sep	1 Oct	2 Oct	3 Oct
MPA-RT daily mean rain rate (mm day^{-1})	23.4	26.8	19.4	16.1	14.2	18.8	14.7	24.3	30.1	29.8	27.4
GPI daily mean rain rate (mm day^{-1})	13.4	17.3	20.5	22.3	23.6	10.0	14.5	13.0	8.3	10.6	4.6
MPA-RT daily volumetric rain (km^3 day^{-1})	23.9	34.6	24.5	19.0	16.1	21.6	14.9	17.5	19.9	18.1	30.6
GPI daily volumetric rain (km^3 day^{-1})	36.5	23.0	27.8	19.9	19.3	29.1	18.5	20.8	17.6	22.0	11.6
MPA-RT mean total rain potential (mm)	34.4	65.4	75.0	47.0	62.6	101.3	76.5	66.4	55.0	44.8	57.6
MPA-RT mean total rain potential for 4 days before landfall								60			
GPI mean total rain potential (mm)	25.5	40.0	82.4	53.2	88.0	47.8	65.3	60.2	23.4	24.0	9.7
GPI mean total rain potential for 4 days before landfall								43			

It can be seen from Fig. 9 that Lili's storm size was much smaller than Isidore's. During its early stage, Lili's daily rain pattern had some asymmetric features, but it became more symmetric after passing over western Cuba on 1 October. During Lili's lifetime, there were two storm total volumetric rain episodes as identified from Fig. 5. From the plan view of Lili's daily rain accumulation shown in Fig. 9, there was a large rain area in the southeast quadrant of the storm, with daily rain accumulation around or larger than 100 mm day^{-1} during the first episode on 24 September. Lili reached tropical storm status on that day. Lili's first mean daily rain-rate maximum was on that day too (Table 1). During Lili's second storm total rain episode on 3 October, the large strong rain area (about 100 mm day^{-1}) was around the storm center extending to a 333-km radius. But the mean daily rain rate over the entire storm on 3 October (27.4 mm day^{-1}) was less than that on 1 October (30.1 mm day^{-1}), when a convective burst occurred. Lili's maximum surface wind reached 64 m s^{-1} early on 3 October, and then rapidly decreased to about 30 m s^{-1} at 1300 UTC 3 October when it made landfall. During Lili's three landfall days (3–5 October), both its total rain accumulation and total rain area were much smaller than those during Isidore's landfall. From Figs. 1c and 1d, the maximum total rain accumulation during Lili's landfall was 100 mm, and the rain also remained more symmetric.

5. Rain potential of Isidore and Lili

The mean total rain potentials derived from MPA-RT rain and best-track data according to (1) as a function of days before landfall of Isidore and Lili are presented in Fig. 10. This rain potential parameter proposed by Griffith et al. (1978) uses both total volumetric rain history and storm translation speed information to predict the storm's flooding potential. It is essentially a crude predictor for the total storm rainfall of a storm and neglects any horizontal rain distribution information. However, the storm total rain potential is a big concern for hurricane landfall precipitation forecasts.

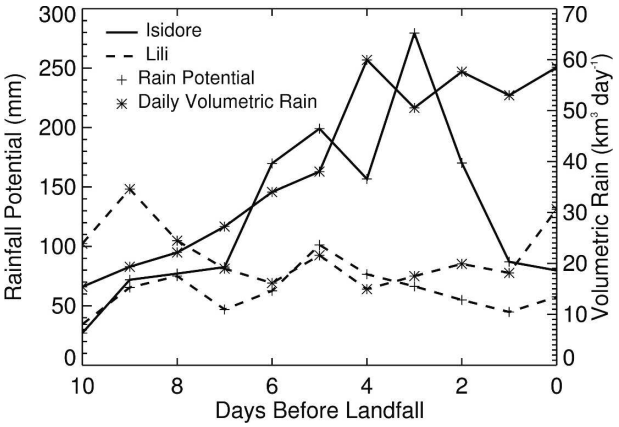

FIG. 10. Comparison of the rainfall potential and daily volumetric rain of Isidore and Lili as a function of days before landfall.

Griffith et al. (1978) used the IR satellite-derived rain estimation in hurricanes to calculate the mean total rain potential for approximately 4 days before landfall (note that the TRaP technique uses 1 day before landfall rain potential as a predictor) for 12 Atlantic tropical storms and hurricanes. They successfully ranked those 12 storms by this calculation and achieved good agreement with actual flooding reports. Despite ignoring the topography, a storm's interaction with midlatitude systems, storm intensity, and detailed rain distribution information, their technique represents a simple but useful method for predicting the flooding potential according to the storm's rainfall history. For the Isidore and Lili cases, the paradox that Isidore produced a large amount of storm total volumetric rain during its landfall as a tropical storm while Lili produced much less volumetric rain during its landfall as a category 1 hurricane was predicted by the large mean total rain potential of Isidore during 1–4 days before its landfall, as is shown in Fig. 10. It is also noted that two peak values of Isidore's rain potential precede the times of maximum volumetric rains.

However, due to the limitation of IR rain estimation, Griffith et al. (1978) can only predict the relative rainfall impacts of 12 tropical cyclones during landfall. Now, with the more accurate MPA-RT product, we may predict the storm rainfall during landfall quantitatively. Table 1 shows the comparison of daily rain parameters and rain potentials derived from the MPA-RT and Geostationary Operational Environmental Satellite (GOES) Precipitation Index (GPI) products for Isidore and Lili. The GPI is a precipitation algorithm that estimates tropical rainfall using IR cloud-top temperature as the sole predictor (Arkin and Meisner 1987). The MPA-RT-derived average total rain potential during the 4 days before landfall for Isidore (Lili) is 173 (60) mm. The rain guage–observed average rainfall for stations around Isidore's (Lili's) landfall point on 26 September (3 October) is 150 (66) mm. However, the GPI-derived average total rain potential during 4 days before landfall for Isidore (Lili) is only 97 (43) mm, indicating an underestimate of about 50%. If we use the MPA-RT-derived 1 day before landfall mean rain potential as a predictor, as in the TRaP technique, the actual landfall rains would also be underestimated substantially for the Isidore and Lili cases. More storms need to be examined to see which time parameters work the best. The larger average rain potential of Isidore during the period of 1–4 days before landfall is largely due to its much larger vortex size, larger volumetric rain, and smaller translation speed. From the rainfall intensity point of view, during the 2 days before landfall (24–25 September for Isidore and 1–2 October for Lili), Lili's MPA-RT daily mean rain rates (30.1 and 29.8 mm day^{-1}, respectively) were even larger than Isidore's (29.9 and 26.9 mm day^{-1}, respectively). However, Lili was smaller and moving faster. Lili's volumetric rain was much smaller than Isidore's volumetric rain (Table 1). From the lifetime rainfall history of both Isidore and Lili, we see that Isidore is inherently a much wetter storm, with much larger daily volumetric rains. Before 22 September, Isidore's rain intensity (indicated by the daily mean rain rate) was large. After that, Isidore's rain intensity decreased but still had a large storm total volumetric rain due to its vortex size expanding.

6. Summary

The 3-h real-time Goddard Multisatellite Precipitation Analysis (MPA-RT) product offers the opportunity to sufficiently monitor the evolution of the precipitation distribution during the entire life cycle of Hurricanes Isidore and Lili (2002). The validation of the high-resolution satellite-based MPA-RT rainfall product using the stage IV NCEP radar and rain gauge Multisensor Precipitation Estimator (MPE IV) product shows that the MPA-RT provides reasonable rain estimates during Isidore and Lili's landfall over the U.S. east coast and is able to quantify the large relative difference in rainfall between these two storms. The MPA-RT-derived rainfall history of Isidore and Lili indicates that the storm total volumetric rainfall amount during their landfall is not well correlated with the storm's intensity, while the storm's inner-core mean rain during each storm's lifetime is. Isidore experienced four rain episodes. The large storm total rain during its landfall was produced mainly by Isidore's strong outer rainbands. Lili experienced much smaller volumetric

rain amounts than Isidore during most of its lifetime. The rain potential derived from the MPA-RT data accurately predicted the large relative difference between Isidore and Lili's storm total rain amount during their landfall. Isidore's mean total rain potential during the 4 days before landfall was almost a factor of 3 higher than that for Lili, while the actual daily volumetric rain of Isidore on its landfall day was almost a factor of 2 higher than that of Lili on its landfall day (see Table 1).

This study also demonstrates that Lili's rapid intensification on early 3 October was related to a strong convective burst on 1 October. This is consistent with previous studies that showed that convective bursts precede the tropical cyclone intensification by approximately 2 days (Rodgers et al. 1994; Rodgers and Pierce 1995).

7. Future work

To first order, the larger diameter of Isidore is responsible for the greater rain volume in a Lagrangian framework, but it is not the only controlling factor. The evaluation of the water vapor budget will give some insight into the important mechanisms that influence the precipitation distribution and storm wetness of Isidore and Lili. The water budget and the crucial environmental factors that influenced the precipitation of Isidore and Lili will be examined by using Navy Operational Global Atmospheric Prediction System (NOGAPS) analyses in detail in (Jiang et al. 2008, Part II of this paper).

The results of this two-part set of papers concern only two storms; the relationships need to be proven by using a large sample of storms. Future work will employ the 7-yr retrospective MPA, NCEP MPE-IV, and NOGAPS analysis datasets for landfall hurricanes over the Atlantic basin. Upon building this database, the MPA estimates can be evaluated for more hurricane events and the rain potential can be associated with the hurricane landfall flooding more quantitatively.

Acknowledgments. The authors thank Drs. Edward J. Zipser and Scott Braun for providing support and valuable comments on this study. Thanks to Drs. Robert Adler and George Huffman for providing MPA-RT data. The authors wish to acknowledge help from Mr. Hal Pierce for processing MPA-RT data. Thanks to Drs. David Roth, John Kobar, and Jeff Hawkins for their assistance on MPE IV and IR satellite data. Thanks are given to Manuel Lonfat for discussion and feedback. The constructive suggestions from three anonymous reviewers resulted in substantial improvements to the manuscript. This research was supported by a NASA TRMM grant. The authors thank Ramesh Kakar (NASA headquarters) for his continued support of TRMM science.

REFERENCES

Adler, R. F., A. J. Negri, P. R. Keehn, and I. M. Hakkarinen, 1993: Estimation of monthly rainfall over Japan and surrounding waters from a combination of low-orbit microwave and geosynchronous IR data. *J. Appl. Meteor.,* **32,** 335–356.

——, G. J. Huffman, and P. R. Keehn, 1994: Global tropical rain estimates from microwave-adjusted geosynchronous IR data. *Remote Sens. Rev.,* **11,** 125–152.

——, ——, D. T. Bolvin, S. Curtis, and E. J. Nelkin, 2000: Tropical rainfall distributions determined using TRMM combined with other satellite and rain gauge information. *J. Appl. Meteor.,* **39,** 2007–2023.

——, and Coauthors, 2003: The version 2 Global Precipitation Climatology Project (GPCP) Monthly Precipitation Analysis (1979–present). *J. Hydrometeor.,* **4,** 1147–1167.

Arkin, P. A., and B. N. Meisner, 1987: The relationship between large-scale convective rainfall and cold cloud over the Western Hemisphere during 1982–84. *Mon. Wea. Rev.,* **115,** 51–74.

Barrett, E. C., 1999: Estimating the amount of rainfall associated with tropical cyclones using satellite techniques. WMO Tech. Doc. Rep. TCO-42, Geneva, Switzerland, 294 pp.

Conner, M. D., and G. W. Petty, 1998: Validation and intercomparison of SSM/I rain-rate retrieval methods over the continental United States. *J. Appl. Meteor.,* **37,** 679–700.

Elsberry, R. L., 2002: Predicting hurricane landfall precipitation. *Bull. Amer. Meteor. Soc.,* **83,** 1333–1340.

——, and F. D. Marks, 1999: The Hurricane Landfall Workshop summary. *Bull. Amer. Meteor. Soc.,* **80,** 683–685.

Ferraro, R., and Coauthors, 2005: The Tropical Rainfall Potential (TRaP) technique. Part II: Validation. *Wea. Forecasting,* **20,** 465–476.

Griffith, C. G., W. L. Woodley, P. G. Gube, D. W. Martin, J. Stout, and D. N. Sikdar, 1978: Rain estimates from geosynchronous satellite imagery: Visible and infrared studies. *Mon. Wea. Rev.,* **106,** 1153–1171.

Heymsfield, G. M., J. B. Halverson, J. Simpson, L. Tian, and T. P. Bui, 2001: ER-2 Doppler radar investigations of the eyewall of Hurricane Bonnie during the Convection and Moisture Experiment-3. *J. Appl. Meteor.,* **40,** 1310–1330.

Huffman, G. J., R. F. Adler, M. Morrissey, D. T. Bolvin, S. Curtis, R. Joyce, B. McGavock, and J. Susskind, 2001: Global precipitation at One-Degree Daily resolution from multisatellite observations. *J. Hydrometeor.,* **2,** 36–50.

——, ——, E. F. Stocker, D. T. Bolvin, and E. J. Nelkin, 2003: Analysis of TRMM 3-hourly multi-satellite precipitation estimates computed in both real and post-real time. Preprints, *12th Conf. on Satellite Meteorology and Oceanography,* Long Beach, CA, Amer. Meteor. Soc., P4.11.

——, and Coauthors, 2007: The TRMM Multisatellite Precipitation Analysis (TMPA): Quasi-global, multiyear, combined-sensor precipitation estimates at fine scales. *J. Hydrometeor.,* **8,** 38–55.

Jiang, H., J. B. Halverson, J. Simpson, and E. J. Zipser, 2008: On the differences in storm rainfall from Hurricanes Isidore and Lili. Part II: Water budget. *Wea. Forecasting,* **23,** 44–61.

Katsanos, D., K. Lagouvardos, V. Kotroni, and G. J. Huffman, 2004: Statistical evaluation of MPA-RT high-resolution precipitation estimates from satellite platforms over the central

and eastern Mediterranean. *Geophys. Res. Lett.,* **31,** L06116, doi:10.1029/2003GL019142.

Kidder, S. Q., and Coauthors, 2005: The Tropical Rainfall Potential (TRaP) technique. Part I: Description and examples. *Wea. Forecasting,* **20,** 456–464.

Kummerow, C., W. S. Olson, and L. Giglio, 1996: A simplified scheme for obtaining precipitation and vertical hydrometeor profiles from passive microwave sensors. *IEEE Trans. Geosci. Remote Sens.,* **34,** 1213–1232.

Lonfat, M., F. D. Marks, and S. S. Chen, 2004: Precipitation distribution in tropical cyclones using the Tropical Rainfall Measuring Mission (TRMM) Microwave Imager: A global perspective. *Mon. Wea. Rev.,* **132,** 1645–1660.

Nesbitt, S. W., E. J. Zipser, and C. D. Kummerow, 2004: An examination of version-5 rainfall estimates from the TRMM Microwave Imager, Precipitation Radar, and rain gauges on global, regional, and storm scales. *J. Appl. Meteor.,* **43,** 1016–1035.

Riehl, H., and J. Malkus, 1961: Some aspects of Hurricane Daisy, 1958. *Tellus,* **13,** 181–213.

Rodgers, E. B., and H. F. Pierce, 1995: Environmental influence on Typhoon Bobbie's precipitation distribution. *J. Appl. Meteor.,* **34,** 2515–2532.

——, J.-J. Baik, and H. F. Pierce, 1994: The environmental influence on tropical cyclone precipitation. *J. Appl. Meteor.,* **33,** 573–593.

——, W. S. Olson, V. M. Karyampudi, and H. F. Pierce, 1998: Satellite-derived latent heating distribution and environmental influences in Hurricane Opal (1995). *Mon. Wea. Rev.,* **126,** 1229–1247.

——, ——, J. Halverson, J. Simpson, and H. F. Pierce, 2000: Environmental forcing of Supertyphoon Paka's (1997) latent heat structure. *J. Appl. Meteor.,* **39,** 1983–2006.

Seo, D. J., 1998: Real-time estimation of rainfall fields using rain gauge data under fractional coverage conditions. *J. Hydrol.,* **208,** 25–36.

Simpson, J., J. B. Halverson, B. S. Ferrier, W. A. Patersen, R. H. Simpson, R. Blakeslee, and S. L. Durden, 1998: On the role of "hot towers" in tropical cyclone formation. *Meteor. Atmos. Phys.,* **67,** 15–35.

Simpson, R. H., 1976: The hurricane disaster potential scale. *Weatherwise,* **27,** 169–186.

Smith, J. A., and W. F. Krajewski, 1991: Estimation of mean field bias of radar rainfall estimates. *J. Appl. Meteor.,* **30,** 397–412.

Spencer, R. W., H. M. Goodman, and R. E. Hood, 1989: Precipitation retrieval over land and ocean with the SSM/I: Identification and characteristics of the scattering signal. *J. Atmos. Oceanic Technol.,* **6,** 254–273.

Weng, F., L. Zhao, R. Ferraro, G. Poe, X. Li, and N. Grody, 2003: Advanced Microwave Sounding Unit cloud and precipitation algorithms. *Radio Sci.,* **38,** 8068–8079.

Zhao, L., and F. Weng, 2002: Retrieval of ice cloud parameters using the Advanced Microwave Sounding Unit. *J. Appl. Meteor.,* **41,** 384–395.